Histol Histopathol (2026) 41: 517-530

Histology and Histopathology
From Cell Biology to Tissue Engineering

ORIGINAL ARTICLE Open Access

USP7 promotes follicular thyroid carcinoma progression and sorafenib resistance by activating NEK2/ATG5-mediated autophagy

Yingcheng Deng[1], Jutao Zeng[2], Hong Cao[2] and Jie Luo[3]

[1]Department of Anatomy, Hunan Traditional Chinese Medical College, Zhuzhou, [2]Department of Breast and Thyroid Surgery, the Second Affiliated Hospital, Hengyang Medical School, University of South China and [3]Department of Anesthesiology, the Second Affiliated Hospital, Hengyang Medical School, University of South China, Hengyang, Hunan, China

Summary. Purpose. To investigate the role of ubiquitin-specific protease 7 (USP7) in thyroid cancer (TC) pathogenesis and sorafenib resistance.

Methods. USP7 expression was compared in normal human thyroid cells and TC cells. The TC line with maximal differential USP7 expression was selected for further study. The functional interaction between USP7 and never in mitosis A (NIMA)-related kinase 2 (NEK2)/autophagy-related 5 (ATG5) was elucidated through a Pearson correlation coefficient analysis and co-immunoprecipitation assay. The half-inhibitory concentration (IC50) of sorafenib in resistant follicular thyroid (FTC) cells was determined following USP7 knockdown and ATG5 overexpression. Furthermore, the effects of USP7 knockdown and the autophagy inducer rapamycin (RAPA) on FTC cell function were assessed by colony formation and Transwell assays. The function of USP7 was validated *in vivo* using a xenograft mouse model, and tumor growth was assessed through gross examination and histopathological staining.

Results. High USP7 expression promoted the proliferation, migration, and invasion of FTC cells and was positively correlated with NEK2 and ATG5 levels. USP7 enhanced NEK2 stability via deubiquitination. Knocking down USP7 downregulated ATG5, and this effect was reversed by NEK2 overexpression. USP7 inhibition reduced the IC_{50} of sorafenib in FTC cells, which was reversed by ATG5 overexpression. USP7 knockdown attenuated FTC cell proliferation, migration, and invasion while increasing the apoptosis rate, and these effects were reversed by RAPA treatment. Knocking down USP7 suppressed the growth of TC xenografts *in vivo*, improved tumor tissue differentiation, and reduced the percentage of Ki-67-positive cells.

Conclusion. USP7 promoted the progression of FTC and induced sorafenib resistance by enhancing NEK2/ATG5-mediated autophagy. This study provides novel insights and potential therapeutic strategies for FTC treatment and overcoming drug resistance.

Key words: Follicular thyroid cancer, USP7, NEK2, Autophagy, Sorafenib resistance

Introduction

Thyroid cancer (TC) is the predominant malignancy of the endocrine system and has experienced a sustained increase in global incidence. Histologically, TC can be classified into differentiated thyroid carcinoma (DTC), anaplastic thyroid carcinoma (ATC), and medullary thyroid carcinoma (MTC) (McLeod et al., 2019; Boucai et al., 2024). Follicular thyroid carcinoma (FTC), a subtype of DTC (Boucai et al., 2024), is characterized by a clinically insidious onset and frequently presents with distant metastases at initial diagnosis (Chen et al., 2022). While most TC patients exhibit favorable prognoses, 10-15% develop radioiodine-refractory DTC (RAIR-DTC), a clinically aggressive subtype associated with therapeutic limitations and markedly reduced five-year survival rates (Wang et al., 2024). Sorafenib, a multi-targeted antiangiogenic kinase inhibitor, constitutes the first-line therapy for progressive DTC following radioactive iodine (RAI) treatment failure (Santos et al., 2019). It primarily inhibits the vascular endothelial growth factor receptors 2/3 (VEGFR2/3), rearranged during transfection (RET) proto-oncogene, and mitogen-activated protein kinase (MAPK) signaling pathways, and has demonstrated synergistic anti-tumor efficacy in

Corresponding Author: Hong Cao, Department of Breast and Thyroid Surgery, the Second Affiliated Hospital, Hengyang Medical School, University of South China, Hengyang 421001, Hunan, PR China. e-mail: 2004020011@usc.edu.cn and Jie Luo, Department of Anesthesiology, the Second Affiliated Hospital, Hengyang Medical School, University of South China, Hengyang 421001, Hunan, PR China. e-mail: luoj0024_usc@163.com

www.hh.um.es. DOI: 10.14670/HH-18-975

combination regimens (Jingtai et al., 2023). Nevertheless, acquired sorafenib resistance substantially compromises clinical outcomes in 30-50% of TC patients within 12 months of treatment initiation (Yi et al., 2018; Run et al., 2021). Therefore, it is critical to elucidate resistance mechanisms and develop novel therapeutic approaches for improving TC management.

Autophagy is a conserved lysosomal degradation pathway that maintains cellular homeostasis through the regulated turnover of organelles and macromolecules (Ichimiya et al., 2020). Apart from its canonical roles in stress adaptation and organelle quality control, autophagy also influences cancer development through oncogenic as well as tumor-suppressive functions (Holm et al., 2022). Studies show that autophagy sustains TC progression by preserving cancer stem cell niches, facilitating epithelial-mesenchymal transition (EMT), and evading apoptotic surveillance (Holm et al., 2022). Yi et al. demonstrated that autophagy inhibition improved the targeted therapeutic efficacy of sorafenib in TC cells (Yi et al., 2018). On the other hand, Lin et al. found that autophagy activation enhanced the anti-proliferative effects of tyrosine kinase inhibitors in MTC cells (Lin et al., 2012).

Ubiquitin-specific protease 7 (USP7) is a deubiquitinating enzyme that is upregulated in various cancers, including breast cancer (Zhang et al., 2020), osteosarcoma (Yang et al., 2024), glioblastoma (Pan et al., 2021), colorectal cancer (An et al., 2017), and lung cancer (Wang et al., 2019). It catalyzes the mono-deubiquitination of SMAD family member 3 (SMAD3), and USP7-mediated positive autoregulation of SMAD3 in p53-deficient lung cancer cells inhibits tumor progression (Huang et al., 2021). X-linked inhibitor of apoptosis protein, a substrate of USP7, also enhances the tumorigenic potential of cancer cells by inhibiting apoptosis (Saha et al., 2022). In addition, USP7 promotes the initiation and metastasis of prostate cancer cells by regulating the stability of the enhancer of zeste homolog 2 (EZH2) (Lee et al., 2020). Elevated USP7 levels in TC cells correlate with unfavorable patient outcomes and autophagy regulation (Xie et al., 2020). There is evidence that USP7 plays a regulatory role in the autophagy pathway (Lu et al., 2021), and USP7 overexpression in osteoporosis models has been shown to enhance autophagic activity and stimulate osteoblast proliferation (Lu et al., 2021). Furthermore, Cui et al. demonstrated that USP7-mediated autophagy regulation governs aging processes in *Drosophila melanogaster* (Cui et al., 2020).

Never in mitosis A (NIMA)-related kinase 2 (NEK2) plays a key role in coordinating centrosome separation during the G2/M phase of the cell cycle, ensuring accurate chromosome segregation (Mardin et al., 2010). It is overexpressed in multiple malignancies (Fang and Zhang, 2016), including cervical cancer (Haiye et al., 2025), and prostate cancer (Zeng et al., 2015), and correlates with advanced tumor phenotypes and poor clinical outcomes. Elevated NEK2 expression promotes the proliferation and metastatic dissemination of neoplastic cells by targeting several intracellular signaling cascades (Xia et al., 2025). For instance, NEK2 modulates autophagic flux in gastric cancer cells by stabilizing Beclin-1 via ubiquitination-dependent mechanisms and enhancing resistance to bortezomib (Xia et al., 2020; Wan et al., 2021). Additionally, Franqui et al. showed that pharmacological inhibition of USP7 attenuated NEK2-mediated drug resistance in myeloma cells (Franqui-Machin et al., 2018).

Based on these findings, we hypothesized that USP7 may promote FTC progression and sorafenib resistance by regulating NEK2-mediated autophagy. This study aimed to elucidate the autophagic mechanisms regulated by USP7 in the malignant progression of FTC.

Materials and methods

Cell culture and treatment

The human normal thyroid cell line Nthy-ori 3-1 (CL-0817, Pricella, China) was maintained in RPMI-1640 (R8758, Sigma, USA) supplemented with 10% fetal bovine serum (FBS; 10099141, Gibco, USA) and 1% penicillin/streptomycin (P/S; C100C5, NCM Biotech, China). The human TC cell line BHT101 (AW-CCH580, Abiowell, China) and human embryonic kidney cell line HEK293T (AW-CNH086, Abiowell, China) were cultured in Dulbecco's modified eagle medium (DMEM) containing 10% FBS and 1% P/S. The human TC cell line TPC-1 (AW-CCH255, Abiowell, China), K1 (AW-CCH573, Abiowell, China), and FTC-133 (AW-CCH197, Abiowell, China) cells were cultivated in RPMI-1640 (R8758, Sigma, USA) with 10% FBS and 1% P/S. Cultures were maintained at 37°C in a humidified 5% CO_2 incubator (DH-160I, Shanghai Santn, China). According to the experimental requirements, cells were transfected with suitable constructs (see below) and/or treated with 40 nmol/L chloroquine (CQ) (Xia et al., 2020), 5 μmol/L sorafenib (Zhang et al., 2018), and 10 ng/mL rapamycin (RAPA) (Banerjee et al., 2012) for 24 hours.

Cell transfection

All plasmids were equilibrated to 4°C prior to use. The cells were transfected with 3 μg of the respective plasmids with 5 μL Lipofectamine 2000 in 95 μL serum-free RPMI 1640 medium. Following six hours of incubation at 37°C with 5% CO_2, the medium was discarded, and the transfected cells were maintained in a complete growth medium. The following expression vectors (HonorGene, China) were employed: human overexpression (oe)-USP7 (pcDNA3.1-USP7-3×Flag, HG-HO113962), human oe-NEK2 (pcDNA3.1-NEK2-3×Flag, HG-HO002497), human oe-ATG5 (pcDNA3.1-ATG5-3×Flag, HG-HO0048497), and the respective negative controls (oe-NC). FTC-133 and HEK293T cells were transfected with USP7-targeting siRNA (si-USP7;

HG-SH003470), and USP7-targeting lentivirus (sh-USP7; HG-LVSH003470).

Western blotting

The protein fraction was extracted from 0.025 g tissue or cell pellets following standardized protocols. Tissue specimens were homogenized in 300 μL ice-cold RIPA buffer (P0013B, Beyotime, China) using a BioPrep-24 homogenizer until complete lysis. Cell pellets were lysed in 200 μL RIPA buffer. The lysates were incubated on ice for 10 minutes and then centrifuged at 12,000g for 15 minutes at 4°C (H1650R, Hunan Xiangyi). The protein concentration in each sample was determined by the BCA method. For immunoblotting, 200 μL protein lysate was mixed with 50 μL 5×Laemmli buffer and denatured at 95°C for 5 minutes. Sodium Dodecyl Sulfate-Polyacrylamide Gel Electrophoresis (SDS-PAGE) separated the protein sample and then transferred it to nitrocellulose (NC) membranes through semi-dry transfer. The membranes were blocked with 5% non-fat milk (P1622, Beijing Pulley) on a shaker for 90 minutes and incubated overnight with the primary antibodies (see Table 1 for dilutions) in 1×PBST at 4°C. After washing thrice with Tris-buffered saline with Tween® 20 (TBST) (10 minutes per wash), the membranes were incubated with horseradish peroxidase (HRP)-conjugated goat anti-mouse IgG (AWS0001-1, 1:5000, Proteintech) and goat anti-rabbit IgG (WS0002-1, 1:6000, Proteintech). Following three 15-minute washes with TBST, the bands were developed using an enhanced chemiluminescent (ECL) reagent (K-12045-D50, Advansta, USA) and imaged on a ChemiScope6100 system (Qinxiang, China).

Co-immunoprecipitation (Co-IP) and Immunoprecipitation (IP)

The suitably cultured cells were washed once with ice-cold phosphate-buffered saline (PBS) and lysed with 600 μL of IP lysis buffer. The suspension was sonicated for 1.5 minutes and incubated on ice for 30 minutes. Lysates were centrifuged at 12,000 rpm for 15 minutes at 4°C, and the supernatants were transferred to fresh 1.5 mL microcentrifuge tubes. For IP, 2.5 μg antibodies against the bait proteins (USP7, Flag, NEK2) or control rabbit IgG (B900610, Proteintech, USA) were added to separate aliquots of each sample, and the samples were incubated overnight at 4°C. Concurrently, 20 μL protein A/G agarose beads were resuspended in 200 μL IP lysis buffer, centrifuged at 3000 rpm for 3 minutes, and the supernatant was discarded. The antibody-lysate complexes and the pre-treated protein A/G beads were incubated, and the beads were rigorously washed four times with 400 μL IP lysis buffer. Following centrifugation, the precipitated proteins were eluted and analyzed by immunoblotting using antibodies listed in Table 1. Ubiquitinated NEK2 (Ub-NEK2) levels were detected by western blotting following IP. The immunoprecipitated complexes were probed through western blotting using a ubiquitin-specific monoclonal antibody (10201-2-AP, Proteintech, USA).

Reverse Transcription-Quantitative Polymerase Chain Reaction (RT-qPCR)

Total RNA was isolated from cultured cells using the TRIzol reagent (15596026, Thermo Fisher, USA), and the purity and concentration were determined spectrophotometrically (A260/A280 ratio ≥1.8) using a Nanodrop UV-Vis system. First-strand cDNA synthesis was performed with 1 μg total RNA using the PrimeScript RT reagent Kit (CW2569, CWBIO, China) under the following conditions: 50°C for 50 minutes followed by 85°C for 5 minutes. RT-qPCR was conducted on the QuantStudio 1 System (Applied Biosystems) using the following 30 μL reaction mixture: 2 μL cDNA template, 1 μL forward primer (10 μM), 1 μL reverse primer (10 μM), 15 μL 2× SYBR Green PCR Master Mix,11 μL nuclease-free water. The cycling parameters were as follows: initial denaturation at 95°C for 10 minutes, 40 cycles of denaturation at 95°C for 15 seconds, and annealing/extension at 60°C for 30 seconds. Relative mRNA expression levels were calculated using the comparative threshold cycle ($2^{-\Delta\Delta Ct}$)

Table 1. List of primary antibodies.

Name	Dilution rate	Source	Cat. number	Company	Country
USP7	1:10000	Mouse	66514-1-Ig	Proteintech	USA
NEK2	1:1000	Rabbit	24171-1-AP	Proteintech	USA
ATG5	1:10000	Rabbit	ab108327	Abcam	UK
LC3	1:3000	Rabbit	14600-1-AP	Proteintech	USA
p62	1:10000	Mouse	66184-1-Ig	Proteintech	USA
Beclin1	1:2000	Rabbit	11306-1-AP	Proteintech	USA
p-mTOR	1:5000	Rabbit	ab109268	Abcam	UK
mTOR	1:10000	Rabbit	ab134903	Abcam	UK
β-actin	1:5000	Rabbit	AWA80002	Abiowell	China
GFP	1:500	Rabbit	SAB4301138	Sigma	USA
Flag	1:1000	Mouse	M8823	Mi1lipore	USA

method and normalized to β-actin. Three technical replicates were analyzed for each sample. The primer sequences are listed in Table 2.

Immunofluorescence

The tissue sections were fixed in 4% paraformaldehyde (N1012, NCM Biotech, China) for 30 minutes at room temperature (RT), washed six times with PBS (5 minutes for each wash), and permeabilized with 0.3% Triton X-100 in PBS at 37°C for 30 minutes. After washing thrice with PBS (3 minutes per wash), the sections were incubated with 5% BSA (SW3015, Solarbio, China) in PBS at 37°C for 1 hour to block non-specific binding. The sections were washed thrice with PBS (5 minutes per wash) and incubated overnight at 4°C with rabbit anti-USP7 primary antibody (14600-1-AP, Proteintech, USA). Following three 5-minute PBS washes, the sections were incubated with Alexa Fluor 488-conjugated goat anti-rabbit IgG secondary antibody (50 μL/section; AWS0005a, Abiowell, China) at 37°C for 90 minutes away from light. The nuclei were counterstained with DAPI (S2110, Solarbio, China) at RT for 10 minutes, followed by three final 5-minute PBS washes. The sections were sealed with glycerol (10010618, Sinopharm, China) and observed under a fluorescence microscope (BA210T, Motic, China).

Cell colony formation assay

Log-phase cells were trypsinized and seeded in six-well plates at a density of 200 cells/well in 2 mL complete growth medium and cultured for 14-21 days. Once colonies (clusters containing ≥50 cells) were visible, the medium was aspirated, and adherent cells were washed twice with PBS. The cells were fixed with 4% paraformaldehyde for 15 minutes at RT, and then stained with 1 mL 0.1% crystal violet (C0121, Beyotime, China) for 30 minutes. The excess stain was removed by washing gently with PBS under laminar flow. Air-dried plates were photographed, and the colonies were counted under a microscope. The experiment was repeated thrice.

Transwell assay

The cells were seeded in the upper chambers of Transwell inserts (3428, Corning, USA) at a density of 2×10^6 cells/mL in 100 μL serum-free RPMI-1640 medium. For the invasion assay, the upper chamber in each well was pre-coated with 200 μg Matrigel in 100 μL serum-free medium for 30 minutes at 37°C. For both the migration and invasion assays, the lower chambers were filled with 500 μL of 10% FBS-containing medium. The chambers were then incubated at 37°C for 48 hours, washed three times with PBS to remove the non-migrating cells, fixed with 4% paraformaldehyde for 20 minutes, and stained with 0.1% crystal violet for 5 minutes. The membranes were transferred onto slides, and cells on the upper surface were observed under an inverted microscope (BA410T, Motic, China). Cells were counted in three random fields of each membrane.

Cell Counting Kit-8 (CCK-8) assay

Cells in the logarithmic growth phase were seeded in 24-well plates at a density of 5×10^3 cells/well in 300 μL medium, and triplicate wells were set up for each condition. Once the cells adhered, the medium was replaced with 300 μL fresh medium containing 10% CCK-8 working solution (30 μL CCK-8 reagent per well). The plates were incubated at 37°C for 4 hours, and the optical density (OD) at 450 nm was measured using a microplate reader.

Apoptosis assay

The suitably treated cells were harvested using EDTA-free trypsin (C100C1, NCM Biotech, China), washed with PBS, and resuspended in 100 μL of resuspension buffer provided in the apoptosis detection kit (KGA1030, KGI Bio, USA). After adding 500 μL binding buffer, the cells were sequentially incubated with 5 μL Annexin V-APC and 5 μL propidium iodide (PI) for 10 minutes at RT in the dark. The stained cells were analyzed within 1 hour using a flow cytometer (A00-1-1102, Beckman, USA).

Animal experiments

Four-week-old male nude mice (13-15 g) were obtained from Hunan SJA Laboratory Animal Co., Ltd (China) and acclimatized for one week under controlled conditions (20-24°C temperature, 40-50% relative humidity) with a 12-hour light/dark cycle. To establish TC xenografts, each mouse was subcutaneously injected

Table 2. Primer sequences.

Primer	Forward 5'-3'	Reverse 5'-3'
H-USP7	ATGCAGAGATGGCTGGGAAC	CTCAGGGCCACATTCCCATT
H-NEK2	AGGAGGGGATCTGGCTAGTG	CAGGGCCAGAGTCAACTGAG
H-ATG5	AAAGATGTGCTTCGAGATGTGT	CACTTTGTCAGTTACCAACGTCA
H-LC3	GAGGAGGGGACTCCATGGCT	TTACAGCGGTCGGCTGGG
H-p62	CCCGTCTACAGGTGAACTCCA	CTCCGATGTCATAGTTCTTGGTC
H-β-actin	ACCCTGAAGTACCCCATCGAG	AGCACAGCCTGGATAGCAAC

with 5×10^6 sh-NC and sh-USP7 FTC-133 cells in 150 μL PBS into the right abdominal quadrant (He et al., 2021). Tumor dimensions and body weight were monitored at four- and three-day intervals, respectively. The animals were humanely euthanized six weeks post-inoculation, and the tumors were excised and photographed. Tumor volume was calculated as $(\text{width})^2\times\text{length}/2$, with length being the longest diameter and width being the shortest diameter perpendicular to the length. All experimental procedures and animal handling were performed with the approval of the Animal Care and Use Committee of the Hunan Traditional Chinese Medical College, in accordance with the National Institutes of Health Guide for the Care and Use of Laboratory Animals.

Hematoxylin-Eosin (H&E) staining

The paraffin-embedded tumor tissue sections were dried at 60°C for 12 hours, cleared in xylene for 20 minutes (three times), rehydrated through graded ethanol (W990001-1, Tianjin Zhiyuan Chemical Co., Ltd., China) series (100, 95, 85, and 75%; 5 minutes each), and rinsed in deionized water for 5 minutes. The sections were immersed in hematoxylin staining solution for 1-10 minutes, rinsed with distilled water, immersed in PBS, and counterstained with eosin for 1-5 minutes. Following dehydration in alcohol for 5 minutes, the sections were cleared in xylene for 10 minutes and covered with neutral resin (G8590, Solarbio, China) for microscopic analysis.

Immunohistochemistry (IHC)

The tissue sections were rinsed in distilled water for 5 minutes, and immersed in a mixture of 0.01 M sodium citrate (C1013, Solarbio, China) and antigen recovery solution (P0083, Beyotime, China). The solution was heated to boiling for 20 minutes in a microwave oven (MM721AAU-PW, Midea, China). The sections were cooled, washed thrice with PBS (3 minutes each time), and incubated with 1% periodic acid for 15 minutes to block endogenous peroxidase activity. After washing thrice with PBS (3 minutes each time), the sections were incubated overnight with anti-Ki-67 primary antibody (1:200; AWA10320, Abiowell, China) at 4°C. The sections were rinsed three times with PBS (5 minutes each time) and incubated with 50-100 μL HRP-conjugated anti-rabbit IgG polymer (undiluted) at 37°C for 30 minutes. The color was developed using 50-100 μL DAB chromogen (ZLI-9019, ZSGB-BIO, China) for 1-5 minutes at RT, and the reaction was terminated by adding distilled water. After counterstaining with hematoxylin (G1100, Solarbio, China) for 5-10 minutes, the sections were rinsed with distilled water, dehydrated using graded ethanol (5 minutes per concentration), and cleared in xylene for 10 minutes. The stained sections were sealed and analyzed microscopically using Image-Pro-Plu 6.0 software.

Statistical analysis

Data were analyzed with GraphPad Prism 8.0. Normally distributed data were presented as mean ± standard. Student's t-test was used to compare two groups, and one-way and two-way ANOVAs were performed for multi-group comparisons. Pearson correlation analysis was performed to assess the correlation between USP7 and NEK2/ATG5. Each experiment was repeated thrice, and $p<0.05$ was considered statistically significant.

Results

High USP7 expression in TC cells was associated with autophagy

USP7, NEK2, ATG5, and LC3II/I were significantly upregulated, while p62 was downregulated in multiple TC cell lines (K1, TPC-1, BHT101, and FTC-133) compared with normal thyroid cells (Nthy-ori 3-1). Among the TC cell lines, FTC-133 exhibited the highest expression levels of these markers (Fig. 1A-C) and was therefore selected for subsequent experiments. Pearson correlation analysis indicated a positive correlation between USP7 expression and NEK2/ATG5 levels (Fig. 1D), suggesting that USP7 upregulation in TC cells may regulate autophagy.

USP7 activated autophagy via the mTOR pathway in FTC cells

To further investigate the mechanistic relationship between USP7-mediated autophagy regulation and TC progression, we knocked down USP7 in FTC-133 cells using three distinct siRNA constructs. RT-qPCR and western blotting demonstrated significant USP7 suppression in all siRNA-treated groups (si-USP7#1, #2, #3) compared with the si-NC group. si-USP7#3 showed the highest silencing efficiency (Fig. 2A) and therefore was selected for subsequent experiments. Notably, USP7 knockdown decreased the expression of ATG5, Beclin-1, and the LC3II/I conversion ratio, while simultaneously increasing phosphorylated mTOR (p-mTOR)/mTOR and p62 accumulation compared with the si-NC group (Fig. 2B). Taken together, USP7 activated autophagy via the mTOR pathway in FTC cells.

USP7 promoted FTC progression by stabilizing NEK2 through ubiquitination-dependent autophagy regulation

We established a stable USP7-overexpressing FTC-133 cell line and treated the cells with CQ to inhibit autophagy. Overexpression of USP7 significantly enhanced the proliferation, migration, and invasion of TC cells compared with control (oe-NC) cells. However, treatment with CQ significantly attenuated the pro-tumorigenic effects of USP7 (Fig. 3A,B). To identify novel molecular partners of USP7 in FTC progression,

we analyzed the interaction of USP7 with the autophagy regulator NEK2. Transient transfection in HEK293T cells demonstrated USP7-NEK2 complex formation (Fig. 3C). The endogenous interaction between these two proteins was confirmed in FTC-133 cells via Co-IP assays (Fig. 3D). Consistent with this, both USP7 and NEK2 proteins were upregulated in the oe-USP7 group compared with the oe-NC group (Fig. 3E,F). As shown in Figure 3G, USP7 overexpression significantly attenuated NEK2 ubiquitination. To further investigate USP7-mediated regulation of NEK2 protein stability, oe-NC and oe-USP7 FTC-133 cells were treated with cycloheximide (CHX; 10 μg/mL) for varying durations (0, 2, 4, and 6 hours). USP7 overexpression reduced the degradation of NEK2 protein under CHX treatment and stabilized the NEK2 protein (Fig. 3H,I). In conclusion, these results confirm that USP7 promoted deubiquitination and stabilization of NEK2.

USP7 activated ATG5-mediated autophagy in FTC cells by upregulating NEK2

To further explore the USP7-NEK2 regulatory axis in FTC, we knocked down USP7 and overexpressed NEK2 in the FTC-133 cells. IP analysis revealed that, compared with the si-NC group, the levels of input-USP7, NEK2, LC3II/I, ATG5, and Beclin-1 were downregulated in the si-USP7 group, while p62, p-mTOR/mTOR, and Ub-NEK2 levels were upregulated. Furthermore, the expression levels of NEK2, ATG5 and Beclin-1, and the LC3II/I ratio were elevated, while p62, p-mTOR/mTOR, and Ub-NEK2 were downregulated in the si-USP7+oe-NEK2 group compared with the si-USP7+oe-NC group (Fig. 4A). These results suggest that USP7 activates ATG5-mediated autophagy by upregulating NEK2. In line with this hypothesis, we observed a significant reduction in the fluorescence intensity of LC3 and autophagy puncta in the si-USP7 group compared with the si-NC group, which was rescued by NEK2 overexpression (Fig. 4B). Furthermore, USP7 knockdown substantially impaired the proliferation, migration, and invasion of FTC cells relative to the si-NC group. Notably, these phenotypic deficits were partially reversed through NEK2 overexpression (Fig. 4C-E). Taken together, USP7 fostered the proliferation, migration, and invasion of FTC cells by activating ATG5-mediated autophagy via NEK2 upregulation.

USP7/NEK2/ATG5-mediated autophagy enhanced FTC malignancy and sorafenib resistance

To further explore the regulatory role of USP7 in NEK2/ATG5-mediated autophagy, we simultaneously knocked down USP7 and overexpressed ATG5 in sorafenib-resistant TC cells. As shown in Figure 5A, ATG5 and Beclin-1 were upregulated, the LC3II/I ratio was increased, and p62 and p-mTOR/mTOR levels were reduced in the si-USP7+oe-ATG5 cells compared with si-USP7+oe-NC controls. Emerging evidence indicates that autophagy may drive tumor progression and chemoresistance (Usman et al., 2021; Pan et al., 2023). To delineate the USP7-autophagy interplay in sorafenib resistance, we conducted dose-response assays (0-10

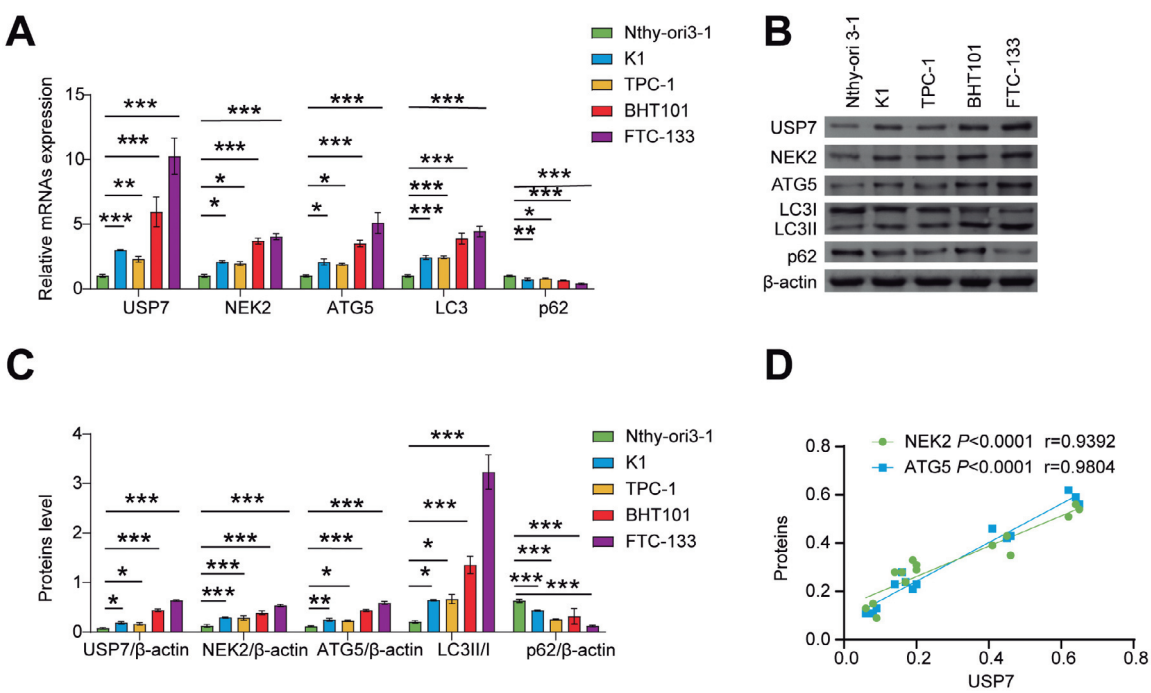

Fig. 1. High USP7 expression in TC cells was associated with autophagy. **A.** The expression levels of USP7, NEK2, ATG5, and LC3II/I mRNAs in the indicated cell lines. **B, C.** Western blotting showing the expression levels of USP7, NEK2, ATG5, and LC3II/I proteins in the indicated cell lines. **D.** Correlation between USP7 and NEK2/ATG5. **p*<0.05, ***p*<0.01, ****p*<0.001. The experiment was repeated thrice.

μmol/L sorafenib) following USP7 knockdown and ATG5 overexpression. Pharmacodynamic profiling demonstrated a marked decrease in cell viability and IC50 values in si-USP7 cells compared with the si-NC group. Conversely, ATG5 overexpression restored both parameters, effectively rescuing the USP7 knockdown phenotype (Fig. 5B). To further validate the association between USP7 and sorafenib sensitivity, FTC-133 cells were treated with increasing doses of sorafenib (0-10 μmol/L). As shown in Fig. 5C, the expression levels of USP7, NEK2, and ATG5 peaked when exposed to 5-10 μmol/L sorafenib, and no significant differences were observed between the dose groups. Consequently, 5 μmol/L was selected for subsequent mechanistic studies.

To elucidate the therapeutic implications of USP7/NEK2/ATG5 axis inhibition in sorafenib-resistant TC, we treated the cells with RAPA, which induces autophagy by inhibiting the mTOR signaling pathway. Compared with the control group, the proliferation, migration, and invasion capabilities were reduced, and apoptosis rates were elevated in the si-USP7 and sorafenib groups. Strikingly, the combination of si-USP7 and sorafenib demonstrated enhanced anti-tumor efficacy over individual interventions (Fig. 5D,E). However, RAPA treatment partially abrogated the anti-tumor effects of USP7 knockdown and sorafenib. As shown in Figure 5F, the proliferative, migratory, and invasion capacities were restored, and apoptosis was inhibited in the si-USP7+sorafenib+RAPA group relative to the si-USP7+sorafenib group. These results confirmed that USP7/NEK2/ATG5-mediated autophagy enhanced sorafenib resistance in FTC cells, promoted malignant behavior, and inhibited apoptosis.

USP7/NEK2/ATG5 axis drives FTC progression in vivo

The oncogenic function of USP7 was validated *in vivo* through the FTC-133 xenograft model. Tumor volume and mass were markedly reduced in the sh-USP7 group compared with the sh-NC group (Fig. 6A,B), while no significant differences were observed between the body weight of tumor-bearing mice from both groups (Fig. 6C). Furthermore, the expression levels of USP7, NEK2, ATG5, and the LC3II/I ratio were downregulated in sh-USP7 tumor tissues, while p62 and p-mTOR/mTOR levels were upregulated compared with the sh-NC group (Fig. 6D). Histopathological analyses revealed enhanced tumor differentiation and lower Ki-67-positive rate in the sh-USP7 group relative to the sh-NC group, indicating that USP7 promotes FTC progression *in vivo* (Fig. 6E-G). Collectively, these results demonstrated that the USP7/NEK2/ATG5 axis drove FTC progression *in vivo*.

Discussion

The prevalence of TC has increased rapidly over recent decades, placing a heavy burden on global healthcare systems (Jianyong et al., 2018; Siraj et al., 2020; Thiesmeyer et al., 2022). Sorafenib, a multi-kinase inhibitor routinely used in TC treatment, may induce drug resistance in patients, leading to metastasis and recurrence (Chang et al., 2023). Furthermore, sorafenib has been shown to trigger autophagy in liver cancer

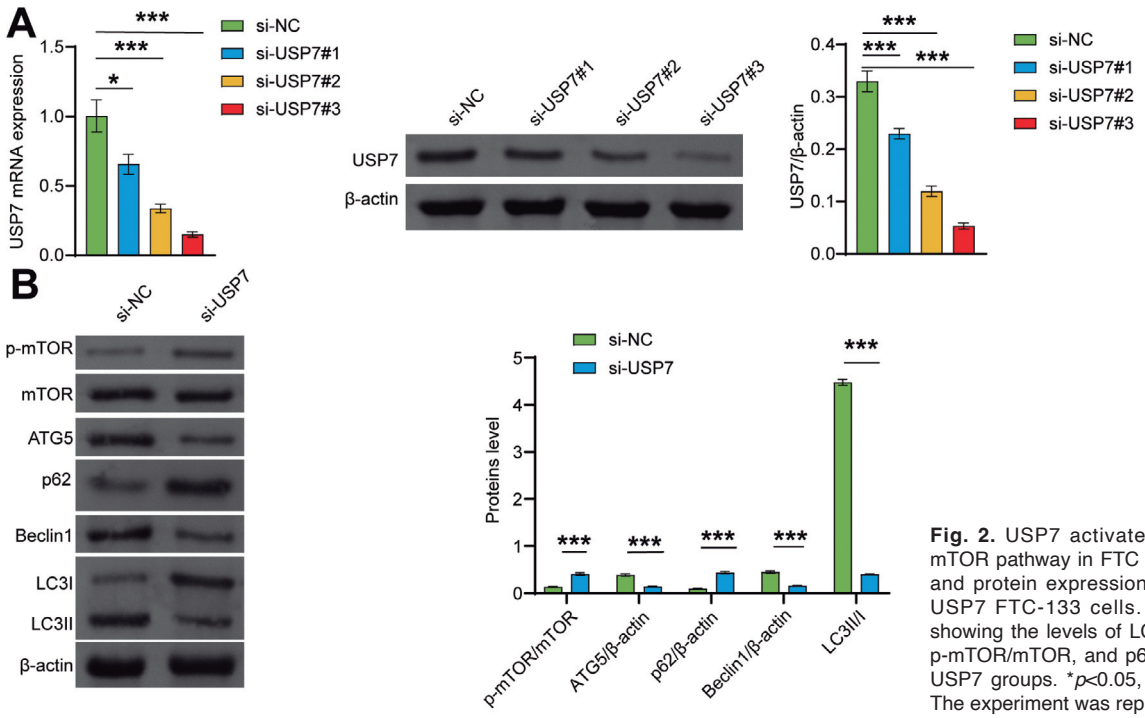

Fig. 2. USP7 activated autophagy via the mTOR pathway in FTC cells. **A.** USP7 mRNA and protein expression in the si-NC and si-USP7 FTC-133 cells. **B.** Western blotting showing the levels of LC3II/I, ATG5, Beclin-1, p-mTOR/mTOR, and p62 in the si-NC and si-USP7 groups. **p*<0.05, ***p*<0.01, ****p*<0.001. The experiment was repeated thrice.

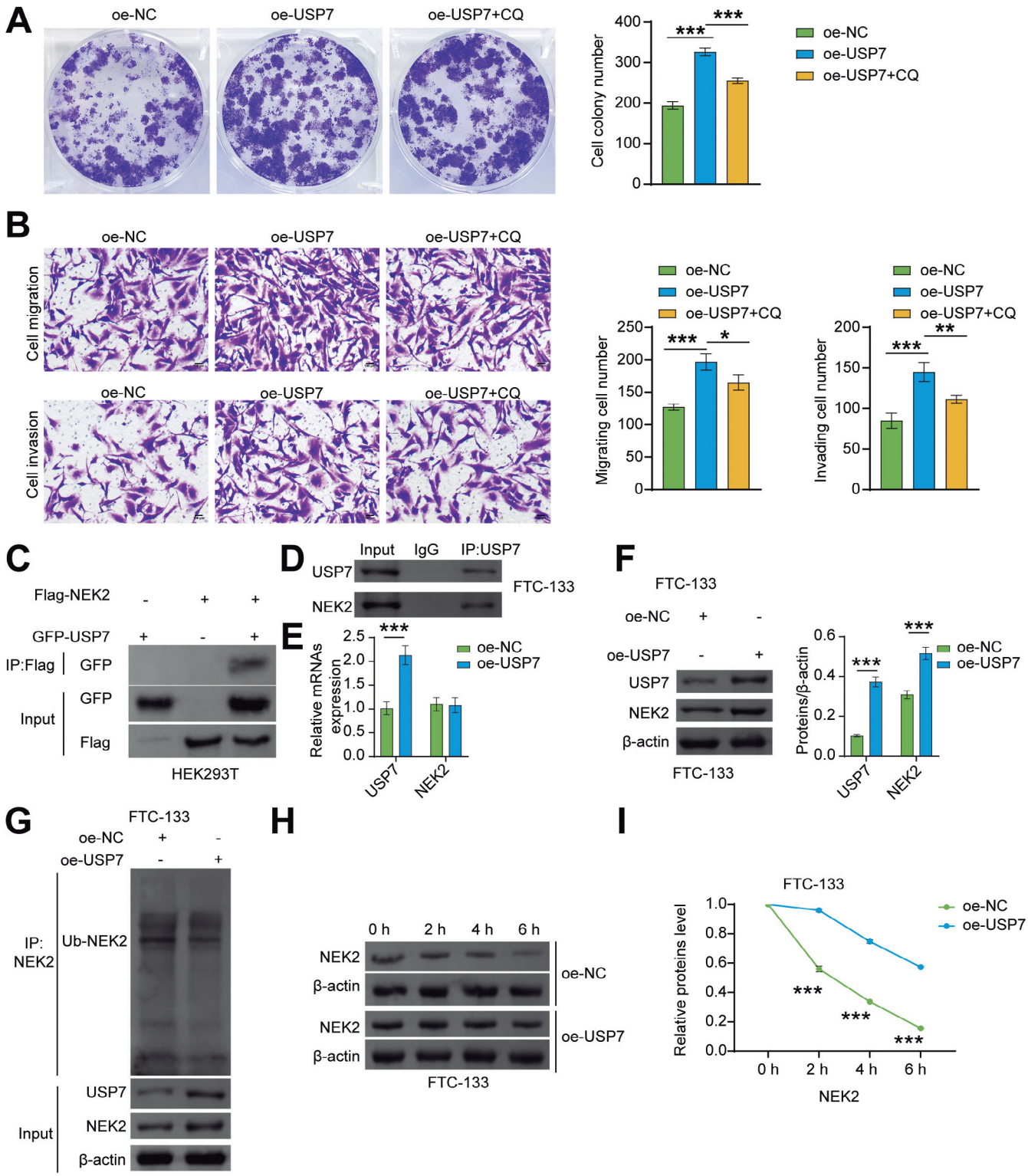

Fig. 3. USP7 promoted FTC progression by stabilizing NEK2 through ubiquitination-dependent autophagy regulation. **A.** The number of colonies formed *in vitro* by the oe-NC and oe-USP7 FTC-133 cells. **B.** Representative images of Transwell assays showing the migration and invasion of FTC-133 cells. Scale bar: 100 μm. **C.** NEK2 protein levels in HEK293T cells transiently transfected with USP7. **D.** Immunoprecipitation of NEK2 in FTC-133 cells using anti-NEK2 or IgG antibodies. **E.** Relative expression of USP7 and NEK2 mRNAs. **F.** Western blotting showing USP7 and NEK2 protein levels. **G.** IP detection of Ub-NEK2, USP7, NEK2, and β-actin expression. **H, I.** Western blotting showing the stability of NEK2 protein in oe-NC and oe-USP7. *p<0.05, **p<0.01, ***p<0.001. The experiment was repeated thrice.

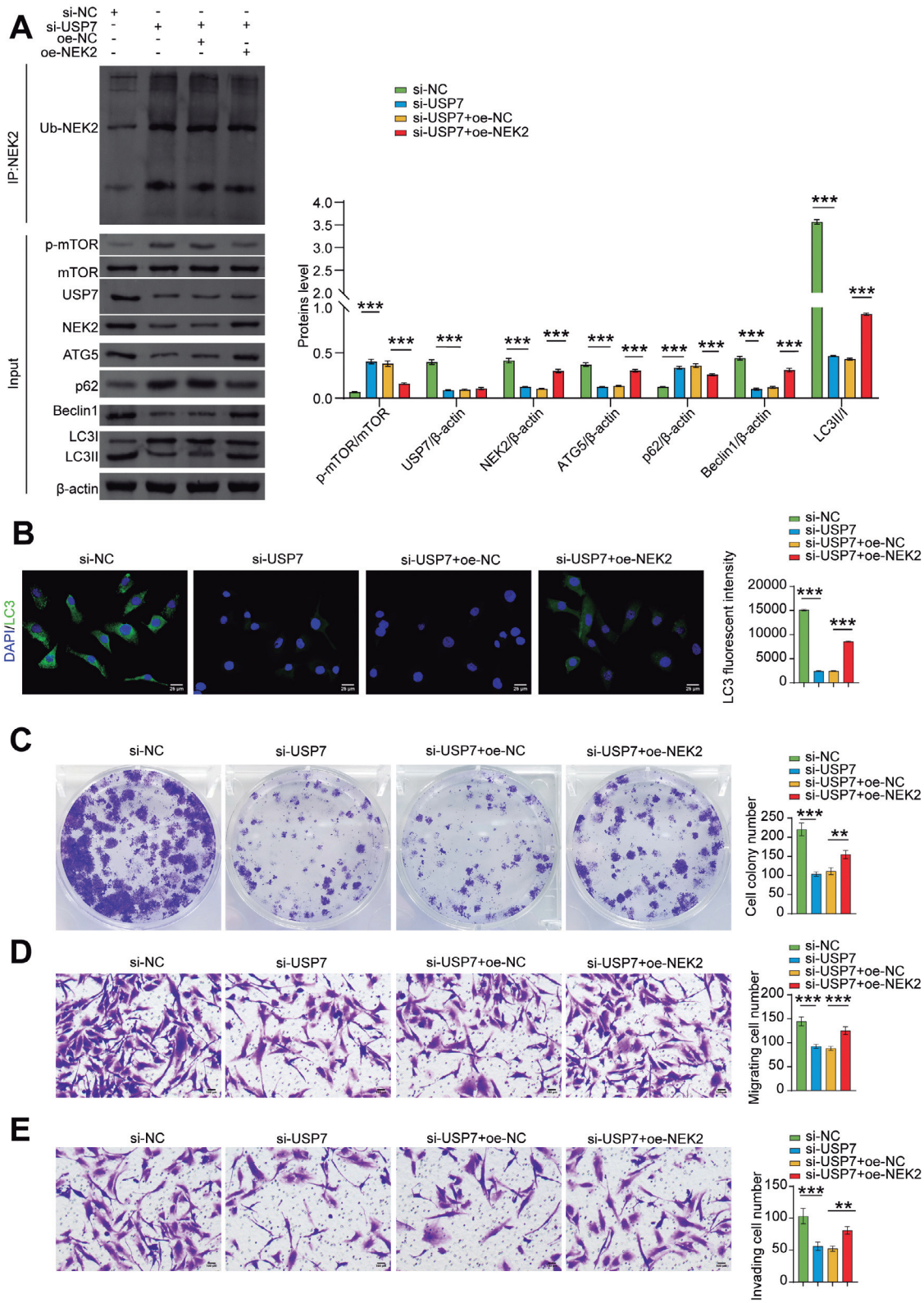

Fig. 4. USP7 activated ATG5-mediated autophagy in FTC cells by upregulating NEK2. **A.** IP detection of NEK2, LC3 II/I, ATG5, Beclin-1, p-mTOR/mTOR, and p62. **B.** Representative immunofluorescence images showing LC3 expression in the si-NC, si-USP7, si-USP7+oe-NC, and si-USP7+oe-NEK2 groups. Scale bar: 25 μm. **C.** Representative images of colonies in the indicated groups. Scale bar: 100 μm. **D, E.** Representative images of Transwell assays showing migration and invasion of TC cells. Scale bar: 100 μm. *p<0.05, **p<0.01, ***p<0.001. The experiment was repeated thrice.

cells, which rendered them insensitive to death stimuli and led to drug resistance (Prieto-Domínguez et al., 2016). Therefore, sorafenib resistance is likely associated with autophagy. We found that USP7 overexpression promoted the proliferation, migration, and invasion of FTC cells, inhibited apoptosis, and enhanced sorafenib resistance by activating ATG5-mediated autophagy through NEK2 upregulation. These novel findings indicate a critical role of USP7 in the development of sorafenib resistance in FTC and provide valuable insights for targeted therapies.

USP7, a member of the deubiquitinating enzyme family, interacts with several substrates that are crucial for cancer progression, such as mouse double minute 2 homolog (MDM2) and phosphatase and tensin homolog (PTEN) (Sarkari et al., 2010; Pozhidaeva and Bezsonova,

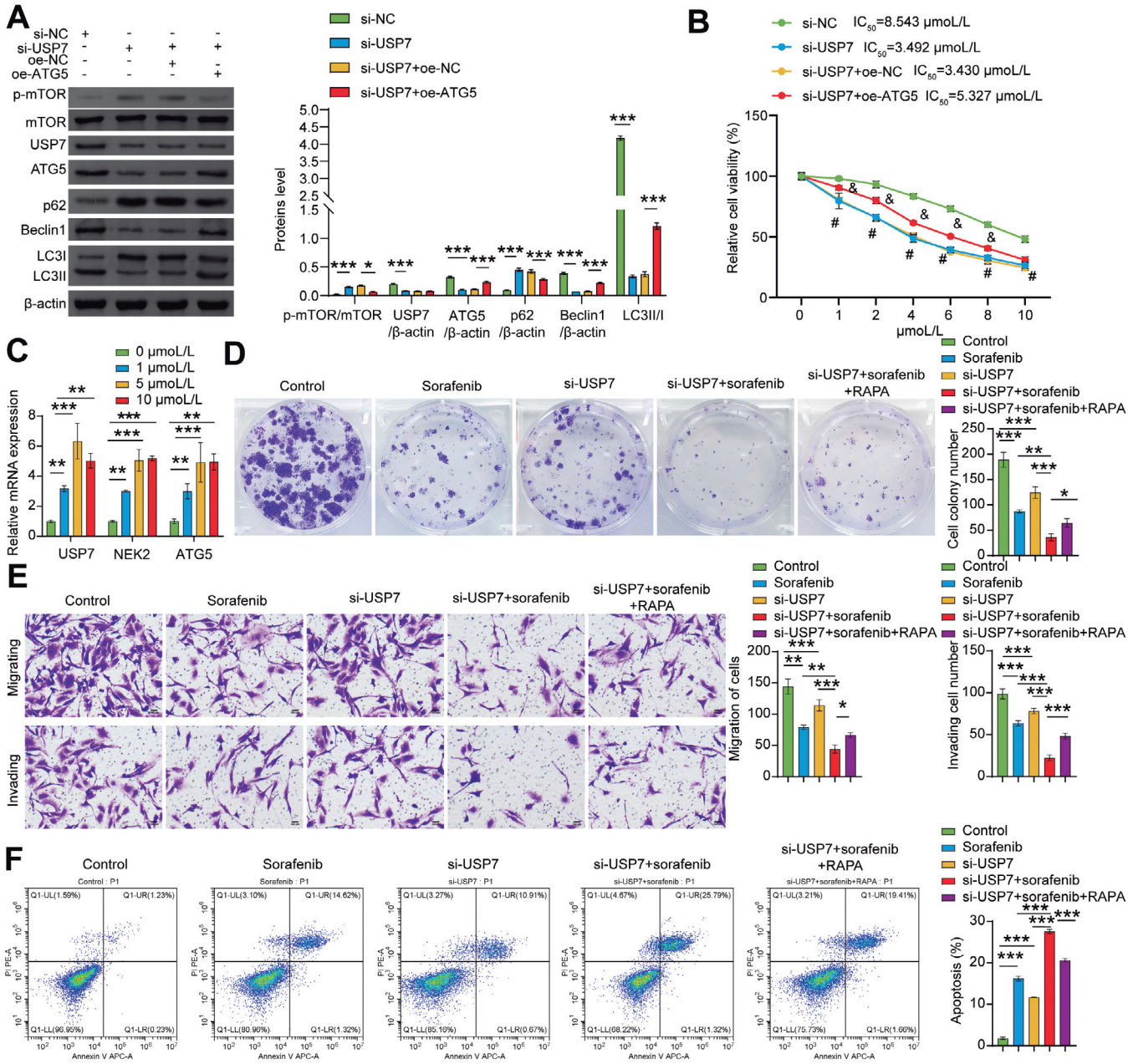

Fig. 5. USP7/NEK2/ATG5-mediated autophagy enhanced FTC malignancy and sorafenib resistance. **A.** Western blotting showing expression levels of USP7, ATG5, LC3II/I, Beclin-1, p-mTOR/mTOR, and p62 in the indicated groups. **B.** Viability of FTC-133 cells treated with different concentrations of sorafenib (0, 1, 2, 4, 6, 8, 10 μmoL/L). **C.** The expression levels of USP7, NEK2, and ATG5 were assessed by RT-qPCR in FTC-133 cells exposed to 0-10 μmol/L sorafenib. **D.** Colony counts in the indicated groups. **E.** Representative images of Transwell assays showing migration and invasion of TC cells. Scale bar: 100 μm. **F.** Apoptosis rates in the indicated groups. *p<0.05, **p<0.01, ***p<0.001. The experiment was repeated thrice.

2019; Nie et al., 2022). Existing studies indicate that USP7 is highly expressed in papillary thyroid carcinoma (PTC) and is significantly associated with unfavorable clinical outcomes (Xie et al., 2020). We found that USP7 expression was increased in TC cells, most significantly in FTC. Currently, there is no literature explicitly reporting the expression of USP7 in FTC. Both PTC and FTC belong to DTC, which represents the most common subtype of TC. Notably, FTC generally exhibits more aggressive biological behavior than PTC (Luvhengo et al., 2023). Based on these observations, we propose that the aberrant expression of USP7 in FTC may contribute to regulating cancer cell invasion and metastatic potential. Functional annotation analyses have revealed significant enrichment of USP7-associated genes in transcriptional regulation, ubiquitin-proteasome processes, DNA repair mechanisms, and cytosolic pattern recognition receptor signaling pathways (Zhang et al.,

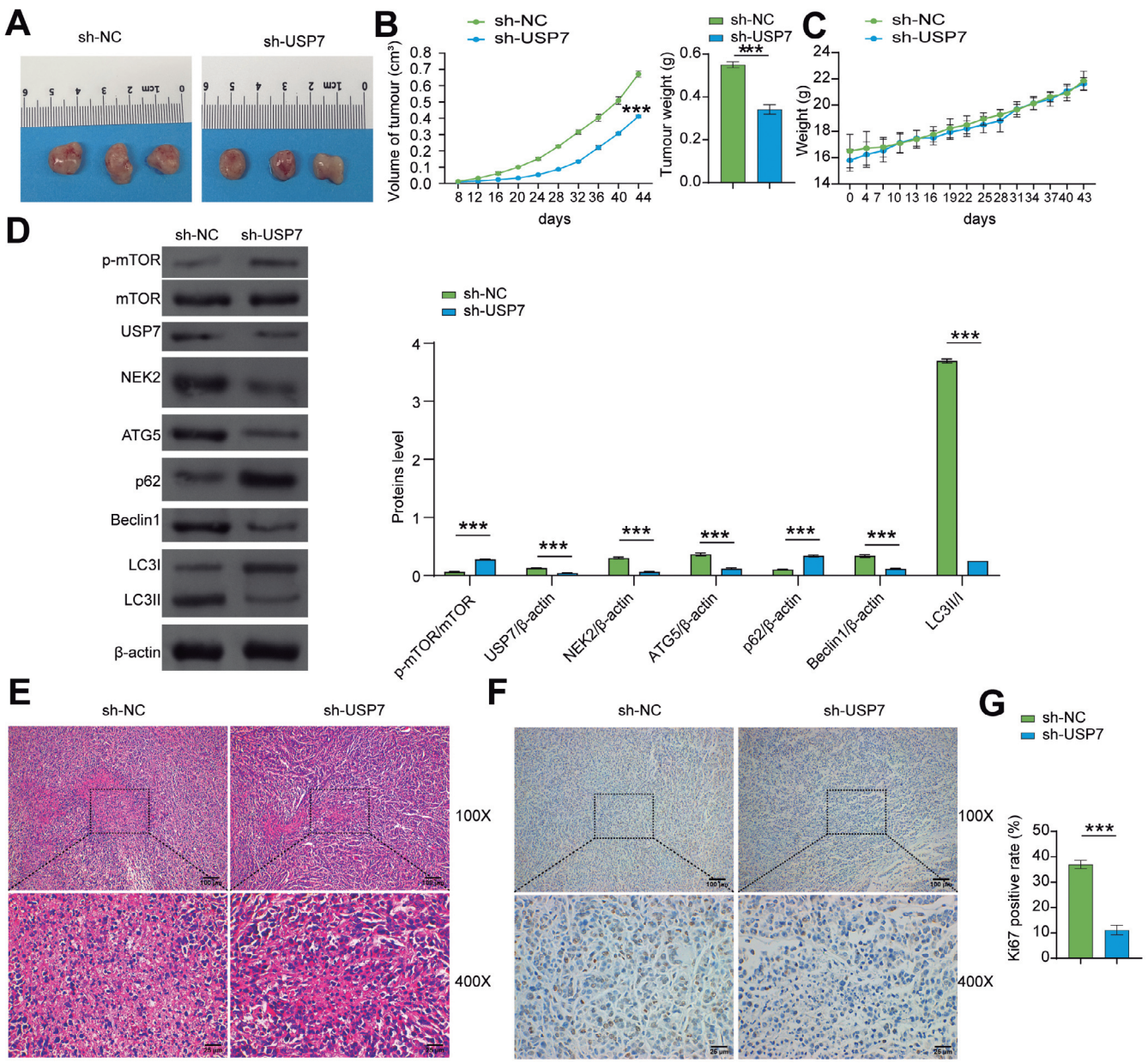

Fig. 6. USP7/NEK2/ATG5 axis drove FTC progression *in vivo*. **A.** Representative images of tumors from the sh-NC and sh-USP7 groups. **B, C.** Changes in tumor volume and body weight in the indicated groups. **D.** Western blotting showing expression of USP7, NEK2, ATG5, LC3II/I, Beclin-1, p-mTOR/mTOR, and p62 in tumor tissues. **E.** Representative images of H&E-stained tumor tissues in the sh-NC and sh-USP7 groups. **F.** Representative IHC images showing Ki-67 expression in the sh-NC and sh-USP7 groups. **G.** Ki-67-positive rate in the sh-NC and sh-USP7 groups. *p<0.05, **p<0.01, ***p<0.001. The experiment was repeated thrice.

2023). Furthermore, USP7 promotes the proliferation of TC cells by directly binding to T-box transcription factor 3 (TBX3) and inhibiting $p57^{KIP2}$ expression through TBX3 deubiquitination and degradation (Xie et al., 2020). In our study, overexpression of USP7 in the FTC cells increased their proliferation, migration, and invasion *in vitr*o and facilitated tumor growth *in vivo*. At the molecular level, USP7 stabilized NEK2 through deubiquitination, thereby activating ATG5-mediated autophagy. Consistent with our findings, Li et al. (2024) demonstrated that USP7 exerts oncogenic effects in TC by stabilizing the fibroblast growth factor receptor 1 (FGFR1) protein through deubiquitination. Thus, USP7 appears to promote FTC progression.

Autophagy supports cancer cell survival, proliferation, and chemoresistance and may even induce drug resistance (Usman et al., 2021; Chen et al., 2025). For instance, compounds targeting unc-51-like kinase 1 (ULK1), a key factor in autophagy initiation, have shown potential in cancer therapy (Liu et al., 2020). Furthermore, stromal sclerosis lowers the sensitivity of pancreatic ductal carcinoma cells to gemcitabine by increasing autophagy levels (Pan et al., 2023). USP7 stabilizes the transcription factor EB (TFEB), a major regulator of autophagy, from proteasomal degradation through deubiquitination (Keshri et al., 2024). Consistent with this, we observed a positive correlation between USP7 expression and autophagy-related proteins like NEK2 and ATG5 in the FTC cells. High NEK2 and ATG5 expression enhanced sorafenib resistance in FTC cells, and promoted their proliferation, migration, and invasion while inhibiting apoptosis. These findings suggest that USP7 is a promising therapeutic target in sorafenib-resistant FTC cells.

NEK2 is a chromosomal instability-associated gene implicated in therapeutic resistance and disease relapse (Xia et al., 2025). Previous studies have demonstrated that binding to USP7 stabilizes NEK2 by preventing its ubiquitination in multiple myeloma (Franqui-Machin et al., 2018). In our study as well, USP7 enhanced the stability of NEK2 by directly interacting with the protein and inhibiting ubiquitination-mediated degradation. Notably, USP7 overexpression significantly upregulated NEK2 expression levels. Furthermore, NEK2 knockdown reversed the effects of USP7 overexpression on the proliferation, migration, and invasion of FTC cells. These results clearly indicate that USP7 promotes FTC progression through NEK2-dependent mechanisms. Since NEK2 has been reported to induce bortezomib resistance in multiple myeloma cells via beclin1-mediated autophagy (Xia et al., 2019), we hypothesized that USP7 may influence sorafenib resistance in FTC cells by modulating autophagy through NEK2. Knocking down USP7 markedly enhanced the sensitivity of FTC cells to sorafenib, and this effect was counteracted by ATG5 overexpression.

While this study delineates the functional role of USP7 in FTC, there are several limitations that warrant acknowledgment. First, given that the significant heterogeneity among FTC subtypes may influence USP7 activity, it is necessary to analyze USP7 expression in other subtypes that were not covered in this study (e.g., undifferentiated 8505C cell line). Secondly, USP7 plays a regulatory role in multiple pathways, including genome stability and protein degradation. Therefore, our results will have to be verified using highly selective inhibitors or CRISPR gene editing technology to rule out the off-target effects of existing USP7 inhibitors. Despite these limitations, our findings propose clinically actionable insights. The development of highly selective USP7 inhibitors targeting its catalytic domain (e.g., the Cys223 active site) should be prioritized, and these inhibitors should be specifically used in biomarker-selected FTC patients with high USP7 expression and autophagy activity. In addition, the therapeutic synergy between USP7 inhibitors and sorafenib could circumvent acquired resistance, while combinatorial approaches employing autophagy modulators might further optimize treatment outcomes. These hypotheses warrant rigorous evaluation in prospective clinical trials, particularly for patients with advanced or sorafenib-refractory FTC. Finally, our findings elucidate the molecular role of the USP7/NEK2/ATG5 axis in autophagy regulation. However, the functional significance of the axis in sorafenib resistance *in vivo* needs more study with sophisticated pharmacological models, which will be a critical focus for subsequent research.

Conclusion

In summary, USP7 promotes FTC progression and sorafenib resistance by activating USP7/NEK2/ATG5 axis-mediated autophagy. Our study identifies this axis as a therapeutic target and provides novel strategies to improve FTC treatment and overcome drug resistance.

Funding. This work was supported by the Clinical Research Center for Breast & Thyroid Disease Prevention in Hunan Province (2018SK4001), the Key Project of Scientific Research Project of Hunan Provincial Department of Education (24A0290), and the Regional Joint Project of the Natural Science Foundation of Hunan Province (2025JJ70127).

Availability of data and materials. The datasets used and analyzed during the current study are available from the corresponding author upon reasonable request.

Conflict of interest. The authors state that there are no conflicts of interest to disclose.

Ethics approval. All experimental procedures and animal handling were performed with the approval of the Animal Care and Use Committee of the Hunan Traditional Chinese Medical College, in accordance with the National Institutes of Health Guide for the Care and Use of Laboratory Animals.

Author Contributions. Y.D.: conceived, designed, experiments, wrote, edited, and commented on the manuscript. J.Z.: data collection and analysis. H.C. and J.L.: conceived, designed, planned the study, checked for problems, and reviewed. J.L.: edited and commented on the manuscript. All authors have accepted responsibility for the manuscript's content and consented to its submission. They have meticulously reviewed all results and unanimously approved the final version of the manuscript.

References

An T., Gong Y., Li X., Kong L., Ma P., Gong L., Zhu H., Yu C., Liu J., Zhou H., Mao B. and Li Y. (2017). Usp7 inhibitor p5091 inhibits wnt signaling and colorectal tumor growth. Biochem. Pharmacol. 131, 29-39.

Banerjee P., Basu A., Wegiel B., Otterbein L.E., Mizumura K., Gasser M., Waaga-Gasser A.M., Choi A.M. and Pal S. (2012). Heme oxygenase-1 promotes survival of renal cancer cells through modulation of apoptosis- and autophagy-regulating molecules. J. Biol. Chem. 287, 32113-32123.

Boucai L., Zafereo M. and Cabanillas M.E. (2024). Thyroid cancer: A review. JAMA 331, 425-435.

Chang H.S., Kim Y., Lee S.Y., Yun H.J., Chang H.J. and Park K.C. (2023). Anti-cancer SERCA inhibitors targeting sorafenib-resistant human papillary thyroid carcinoma. Int. J. Mol. Sci. 24, 7069.

Chen Y.K., Chen Y.C., Lin W.X., Zheng J.H., Liu Y.Y., Zou J., Cai J.H., Ji Z.Q., Chen L.Z., Li Z.Y. and Chen Y.X. (2022). Follicular carcinoma of the thyroid with a single metastatic lesion in the lumbar spine: A case report. World J. Clin. Cases 10, 9493-9501.

Chen C., Jin L., Wan H., Liu H., Zhang S., Shen G., Gong J. and Zhu Y. (2025). TIPE3 promotes drug resistance in colorectal cancer by enhancing autophagy via the USP19/Beclin1 pathway. J. Cell Death Discov. 25, 202.

Cui L., Song W., Zeng Y., Wu Q., Fan Z., Huang T., Zeng B., Zhang M., Ni Q., Li Y., Wang T., Li D., Mao X., Lian T., Yang D., Yang M. and Fan X. (2020). Deubiquitinase USP7 regulates *Drosophila* aging through ubiquitination and autophagy. Aging 12, 23082-23095.

Fang Y. and Zhang X. (2016). Targeting NEK2 as a promising therapeutic approach for cancer treatment. Cell Cycle 15, 895-907.

Franqui-Machin R., Hao M., Bai H., Gu Z., Zhan X., Habelhah H., Jethava Y., Qiu L., Frech I., Tricot G. and Zhan F. (2018). Destabilizing NEK2 overcomes resistance to proteasome inhibition in multiple myeloma. J. Clin. Invest. 128, 2877-2893.

Haiye J., Xiangzhu W., Yunfei Z., Shumin G., Chang N., Yaohui J., Heng Y. and Xinmin N. (2025). Overexpressed NEK2 contributes to progression and cisplatin resistance through activating the Wnt/β-catenin signaling pathway in cervical cancer. Cancer Cell Int. 25, 45.

He J., Zhou M., Yin J., Wan J., Chu J., Jia J., Sheng J., Wang C., Yin H. and He F. (2021). METTL3 restrains papillary thyroid cancer progression via m^{6}A/c-Rel/IL-8-mediated neutrophil infiltration. Mol. Ther. 29, 1821-1837.

Holm T.M., Yeo S., Turner K.M. and Guan J.L. (2022). Targeting autophagy in thyroid cancer: EMT, apoptosis, and cancer stem cells. Front. Cell Dev. Biol. 10, 821855.

Huang Y.T., Cheng A.C., Tang H.C., Huang G.C., Cai L., Lin T.H., Wu K.J., Tseng P.H., Wang G.G. and Chen W.Y. (2021). USP7 facilitates SMAD3 autoregulation to repress cancer progression in p53-deficient lung cancer. Cell Death Dis. 12, 880.

Ichimiya T., Yamakawa T., Hirano T., Yokoyama Y., Hayashi Y., Hirayama D., Wagatsuma K., Itoi T. and Nakase H. (2020). Autophagy and autophagy-related diseases: A review. Int. J. Mol. Sci. 21, 8974.

Jianyong L., Jinjing Z., Zhihui L., Tao W., Rixiang G. and Jingqiang Z. (2018). A nomogram based on the characteristics of metastatic lymph nodes to predict papillary thyroid carcinoma recurrence. Thyroid 28, 301-310.

Jingtai Z., Linfei H., Yuyang Q., Ning K., Xinwei Y., Xin W., Xianhui R., Dongmei H., Weiwei Y., Xiangrui M., Tianze Z., Wei W. and Xiangqian Z. (2023). Targeting Aurora-A inhibits tumor progression and sensitizes thyroid carcinoma to sorafenib by decreasing PFKFB3-mediated glycolysis. Cell Death Dis. 14, 224.

Keshri S., Vicinanza M., Takla M. and Rubinsztein D.C. (2024). USP7 protects TFEB from proteasome-mediated degradation. Cell Rep. 43, 114872.

Lee J.E., Park C.M. and Kim J.H. (2020). USP7 deubiquitinates and stabilizes EZH2 in prostate cancer cells. Genet. Mol. Biol. 43, e20190338.

Li X.B., Li J.L., Wang C., Zhang Y. and Li J. (2024). Identification of mechanism of the oncogenic role of FGFR1 in papillary thyroid carcinoma. Eur. J. Histochem. 68, 4048.

Lin C.I., Whang E.E., Lorch J.H. and Ruan D.T. (2012). Autophagic activation potentiates the antiproliferative effects of tyrosine kinase inhibitors in medullary thyroid cancer. Surgery 152, 1142-1149.

Liu L., Yan L., Liao N., Wu W.Q. and Shi J.L. (2020). A review of ULK1-mediated autophagy in drug resistance of cancer. Cancers 12, 352.

Lu X., Zhang Y., Zheng Y. and Chen B. (2021). The miRNA-15b/USP7/KDM6B axis engages in the initiation of osteoporosis by modulating osteoblast differentiation and autophagy. J. Cell Mol. Med. 25, 2069-2081.

Luvhengo T.E., Bombil I., Mokhtari A., Moeng M.S., Demetriou D., Sanders C. and Dlamini Z. (2023). Multi-omics and management of follicular carcinoma of the thyroid. Biomedicines 11, 1217.

Mardin B.R., Lange C Fau - Baxter J.E., Baxter Je Fau - Hardy T., Hardy T Fau - Scholz S.R., Fry A.M. and Schiebel E. (2010). Components of the Hippo pathway cooperate with nek2 kinase to regulate centrosome disjunction. Nat. Cell Biol. 12, 1166-1176.

McLeod D.S.A., Zhang L., Durante C. and Cooper D.S. (2019). Contemporary debates in adult papillary thyroid cancer management. Endocr. Rev. 40, 1481-1499.

Nie L., Wang C., Liu X., Teng H., Li S., Huang M., Feng X., Pei G., Hang Q., Zhao Z., Gan B., Ma L. and Chen J. (2022). USP7 substrates identified by proteomics analysis reveal the specificity of USP7. Genes Dev. 36, 1016-1030.

Pan T., Li X., Li Y., Tao Z., Yao H., Wu Y., Chen G., Zhang K., Zhou Y. and Huang Y. (2021). USP7 inhibition induces apoptosis in glioblastoma by enhancing ubiquitination of ARF4. Cancer Cell Int. 21, 508.

Pan H., Zhu S., Gong T., Wu D., Zhao Y., Yan J., Dai C., Huang Y., Yang Y. and Guo Y. (2023). Matrix stiffness triggers chemoresistance through elevated autophagy in pancreatic ductal adenocarcinoma. Biomater. Sci. 11, 7358-7372.

Pozhidaeva A. and Bezsonova I. (2019). USP7: Structure, substrate specificity, and inhibition. DNA Repair 76, 30-39.

Prieto-Domínguez N., Ordóñez R., Fernández A., García-Palomo A., Muntané J., González-Gallego J. and Mauriz J.L. (2016). Modulation of autophagy by sorafenib: Effects on treatment response. Front. Pharmacol. 7, 151.

Run L., Wang L., Nong X., Li N., Huang X. and Xiao Y. (2021). Involvement of HMGB1 in vemurafenib resistance in thyroid cancer cells harboring BRAF (V600E) mutation by regulating excessive autophagy. Endocrine 71, 418-426.

Saha G., Sarkar S., Mohanta P.S., Kumar K., Chakrabarti S., Basu M. and Ghosh M.K. (2022). USP7 targets XIAP for cancer progression: Establishment of a p53-independent therapeutic avenue for glioma. Oncogene 41, 5061-5075.

Santos F.S., Santos R.J. and Leite V. (2019). Sorafenib and sunitinib for the treatment of metastatic thyroid cancer of follicular origin: A 7-

year single-centre experience. Eur. Thyroid J. 8, 262-267.

Sarkari F., La Delfa A., Arrowsmith C.H., Frappier L., Sheng Y. and Saridakis V. (2010). Further insight into substrate recognition by USP7: Structural and biochemical analysis of the HdmX and Hdm2 interactions with USP7. J. Mol. Biol. 402, 825-837.

Siraj A.K., Parvathareddy S.K., Qadri Z., Siddiqui K., Al-Sobhi S.S., Al-Dayel F. and Al-Kuraya K.S. (2020). Annual hazard rate of recurrence in middle eastern papillary thyroid cancer over a long-term follow-up. Cancers 12, 3624.

Thiesmeyer J.W., Limberg J., Ullmann T.M., Greenberg J.A., Egan C.E., Moore M., Finnerty B.M., Laird A.M., Zarnegar R., Fahey T.J., 3rd and Beninato T. (2022). Insurance type is associated with appropriate use of surgical and adjuvant care for differentiated thyroid carcinoma. Surgery 171, 140-146.

Usman R.M., Razzaq F., Akbar A., Farooqui A.A., Iftikhar A., Latif A., Hassan H., Zhao J., Carew J.S., Nawrocki S.T. and Anwer F. (2021). Role and mechanism of autophagy-regulating factors in tumorigenesis and drug resistance. Asia Pac. J. Clin. Oncol. 17, 193-208.

Wan H., Xu L., Zhang H., Wu F., Zeng W. and Li T. (2021). High expression of NEK2 promotes gastric cancer progression via activating AKT signaling. J. Physiol. Biochem. 77, 25-34.

Wang Z., Kang W., You Y., Pang J., Ren H., Suo Z., Liu H. and Zheng Y. (2019). USP7: Novel drug target in cancer therapy. Front. Pharmacol. 10, 427.

Wang Y., Lu X. and Liu H. (2024). Current status of the prediction for radio-iodine refractory thyroid cancer: A narrative review. Front. Endocrinol. 15, 1433553.

Xia J., He Y., Meng B., Zhang J., Wu X., Feng X., Kuang C., Guo J., Zhu Y., Lei Q., Guan Y., Shen Y., Qiu L. and Zhou W. (2019). NEK2 promotes bortezomib resistance through enhancing autophagy by upregulation of Beclin1 in multiple myeloma cells. Blood 134 (Suppl. 1), 4332-4332.

Xia J., He Y., Meng B., Chen S., Zhang J., Wu X., Zhu Y., Shen Y., Feng X., Guan Y., Kuang C., Guo J., Lei Q., Wu Y., An G., Li G., Qiu L., Zhan F. and Zhou W. (2020). NEK2 induces autophagy-mediated bortezomib resistance by stabilizing Beclin-1 in multiple myeloma. Mol. Oncol. 14, 763-778.

Xia J., Zhao H., Edmondson J.L., Koss B. and Zhan F. (2025). Role of NEK2 in tumorigenesis and tumor progression. Trends Mol. Med. 31, 79-93.

Xie P., Wang H., Xie J., Huang Z., Chen S., Cheng X., Zhang X., Liu F., Li Y. and Huang D. (2020). USP7 promotes proliferation of papillary thyroid carcinoma cells through TBX3-mediated $p57^{KIP2}$ repression. Mol. Cell. Endocrinol. 518, 111037.

Yang Z., Yu W., Xu A., Liu B., Jin L., Tao H. and Wang D. (2024). mTORC1 accelerates osteosarcoma progression via m6A-dependent stabilization of USP7 mRNA. Cell Death Discov. 10, 127.

Yi H., Ye T., Ge M., Yang M., Zhang L., Jin S., Ye X., Long B. and Li L. (2018). Inhibition of autophagy enhances the targeted therapeutic effect of sorafenib in thyroid cancer. Oncol. Rep. 39, 711-720.

Zeng Y.R., Han Z.D., Wang C., Cai C., Huang Y.Q., Luo H.W., Liu Z.Z., Zhuo Y.J., Dai Q.S., Zhao H.B., Liang Y.X. and Zhong W.D. (2015). Overexpression of NIMA-related kinase 2 is associated with progression and poor prognosis of prostate cancer. BMC Urol. 15, 90.

Zhang K., Chen J., Zhou H., Chen Y., Zhi Y., Zhang B., Chen L., Chu X., Wang R. and Zhang C. (2018). PU.1/microRNA-142-3p targets ATG5/ATG16l1 to inactivate autophagy and sensitize hepatocellular carcinoma cells to sorafenib. Cell Death Dis. 9, 312.

Zhang Q., Cao C., Gong W., Bao K., Wang Q., Wang Y., Bi L., Ma S., Zhao J., Liu L., Tian S., Zhang K., Yang J., Yao Z., Song N. and Shi L. (2020). A feedforward circuit shaped by ECT2 and USP7 contributes to breast carcinogenesis. Theranostics 10, 10769-10790.

Zhang S.Y., Ruan J.J., Jin D.M., Chen N., Xie W.G. and Ruan Q.F. (2023). Pan-cancer analysis of ubiquitin-specific protease 7 and its expression changes in the carcinogenesis of scar ulcer. Zhonghua Shao Shang Yu Chuang Mian Xiu Fu Za Zhi. 39, 518-526 (in Chinese).

Accepted July 31, 2025